poral position of the response window to a shorter or longer value, depending on the subject's ability to perform (for example, shortening it if subjects were making few errors). The response window procedure obliged subjects to respond at speeds that did not permit high levels of accuracy and, consequently, error rates were substantial. (Mean latencies of highly motivated subjects under instructions to respond rapidly are typically between 550 and 650 ms.) The production of relatively high error rates allowed the priming effect—that is, the effect of the prime's congruence versus incongruence with the target's meaning—to be observed in subjects' error rates rather than in their response latencies to targets. With this response window procedure, priming took the form of lower error rates for congruent priming than for incongruent priming, reflecting some combination of facilitation by congruent primes and interference by incongruent primes. Priming was therefore measurable by observing the difference between these error rates. Even though the procedure was designed to constrain response latencies to approximately the range of values that define the response window, response accuracy was analyzed for all trials except for a small percentage with latencies greater than 1500 ms, a value substantially longer than the time elapsed at the end of the window interval. The primary measure used with these data was signal detection theory's *d'* measure of sensitivity of the target word's response to the prime word's meaning [see the further explanation in the legend to Fig. 1, and D. M. Green and J. A. Swets, *Signal Detection Theory and Psychophysics* (Wiley, New York, 1967)]. Results for this sensitivity measure were similar to those obtained with various alternative measures, such as the increase in error rate for incongruent relative to congruent primes or measured information transmitted from prime stimulus to target response. Prime words were presented for 17, 33, or 50 ms at a centered display location to which subjects were instructed to attend. In the visually masked (subliminal) prime condition, the prime was both preceded and followed, at the same screen location, by strings of consonants that served as forward mask (premask) and backward mask (postmask). (An example of a mask stimulus is the letter string GKQHYTPDGFQBYLG.) The premask, prime, postmask, and target stimuli were presented as black letters on a gray background. The premask lasted 100 ms and the postmask 17 ms. (Other pilot studies had shown that masking effectiveness was unaltered by increases in postmask duration beyond 17 ms, the minimum value obtainable with the 60-Hz computer display used in this research.) Subjects viewed the computer video display through a device that presented images from left and right halves of the display screen separately to left and right eyes. Although this dichoptic presentation was not needed for the present procedures (which presented identical stimuli to both eyes at all times), its use has been found to increase mildly the effectiveness of visual masking. The combination of premask and postmask made the prime words difficult or impossible to see for almost all subjects. By contrast, in supraliminal conditions the masking consonant strings were replaced by blanks (that is, the screen background color), as a consequence of which the prime words were easily legible despite their short (50 ms) duration.

12. Because preliminary findings revealed that direct measure performance was depressed by the requirement to respond rapidly, the response window procedure was not used during blocks of trials that obtained direct measures. Different discriminations on visually masked stimuli were requested in different experiments to allow opportunities to demonstrate that some types of information might penetrate visual masking more readily than others. The basic properties of the results shown in Fig. 1 did not vary with the different direct measures, adding to confidence in generality of conclusions.
13. The conclusion that unconscious cognition is indicated by the presence of statistically significant intercept effects in the regression analyses of Fig. 1 rests on a methodological analysis by A. G. Greenwald, M. R. Klinger, and E. S. Schuh [*J. Exp. Psychol. Gen.* **124**, 22 (1995)] that extends the logic of an analysis introduced by P. M. Merikle and E. M. Reingold [*J. Exp. Psychol. Learn. Mem. Cognit.* **17**, 224 (1991)]. A concern in interpreting such intercept effects is the possibility that a spurious intercept may be produced when the predictor (in this instance, the direct measure of prime perceptibility) is imperfectly measured. However, the regression analyses in Fig. 1 do not have the properties that can produce such spurious intercept effects. Such properties include both positive regression slopes and average predictor scores substantially above zero. In contrast, the regression slopes that we obtained were approximately flat and predictor scores (that is, direct measures) were noticeably above zero only with prime duration of 50 ms. For a more detailed discussion of the possibility of spurious intercept effects, see (*21*)
14. The level of perceptibility of masked 50-ms primes can be read from the horizontal distribution of values in the lower panel of Fig. 1, A and C. Levels of direct measure performance corresponding to *d'* values <1.0 are commonly associated with self-reports of little or no perceptibility. Findings of SOA effects closely resembling those in Fig. 2B were obtained when the plotted variable was changed to magnitude of intercept effect from regression analysis; that is, statistically significant intercept effects were found only for the 67-ms SOA. The intercept-effect alternative analysis confirms that the pattern in Fig. 2B for subliminal priming as a function of SOA is indeed a pattern for unconscious priming. The plotted analysis in Fig. 2B, which includes all subjects who received masked priming, is properly comparable to the analysis in Fig. 2A for supraliminal priming (for which regression analysis is not an appropriate method).
15. The result shown in Fig. 3 is related to one previously reported by J. Cheesman and P. M. Merikle [*Can. J. Psychol.* **40**, 343 (1986)]. They showed that supraliminal priming was greater when there was a higher proportion of congruent priming trials in a block of trials, but subliminal priming showed no such effect. Their finding could be explained by the difference in two-trial sequential effects shown in Fig. 3.
16. D. E. Broadbent, *Perception and Communication* (Pergamon, London, 1958); E. C. Cherry, *J. Acoust. Soc. Am.* **25**, 975 (1953); A. M. Treisman, *Q. J. Exp. Psychol.* **12**, 242 (1960).
17. U. Neisser, *Cognitive Psychology* (Appleton-Century-Crofts, New York, 1967). See also G. Sperling, *Acta Psychol.* **27**, 285 (1967); D. A. Norman, *Psychol. Rev.* **75**, 522 (1968). The language of information-processing stages used in this description has now surrendered paradigmatic center stage to neural network models. However, the empirical phenomena captured in this language remain solidly established.
18. The brevity of unconscious semantic activation measured by the prime-target SOA should not be confused with the latency after masked prime presentation at which semantic information is available. Semantic activation is presumed to occur after preliminary operations that may require a few hundred milliseconds for subliminal prime words (as well as for visible target words).
19. G. Sperling, *Psychol. Monogr.* **74**, 11, (1960); T. A. Busey and G. R. Loftus, *Psychol. Rev.* **101**, 446 (1994); V. di Lollo and P. Dixon, *J. Exp. Psychol. Hum. Percept. Perform.* **14**, 671 (1988).
20. M. C. Potter, *Mem. Cognit.* **21**, 156 (1993).
21. A. G. Greenwald and S. C. Draine, in *25th Carnegie Symposium on Cognition: Scientific Approaches to the Question of Consciousness*, J. D. Cohen and J. W. Schooler, Eds. (Erlbaum, Mahwah, NJ, in press).
22. Cubic polynomial regression functions were used to capture possible nonlinear trends in the data. However, it can be seen in the figure that intercept effects for these nonlinear functions were similar to those estimated by linear regression functions.
23. R. L. Abrams, S. C. Draine, A. G. Greenwald, paper presented at the 36th Annual Meeting of the Psychonomic Society, Los Angeles, CA, 10 to 12 November, 1995.
24. Supported by grants from the National Institute of Mental Health (MH-41328) and National Science Foundation (SBR-9422242).

27 February 1996; accepted 25 July 1996

Parallel and Antiparallel $(G{\cdot}GC)_2$ Triple Helix Fragments in a Crystal Structure

Dominique Vlieghe, Luc Van Meervelt, Alain Dautant, Bernard Gallois, Gilles Précigoux, Olga Kennard*

Nucleic acid triplexes are formed by sequence-specific interactions between single-stranded polynucleotides and the double helix. These triplexes are implicated in genetic recombination in vivo and have application to areas that include genome analysis and antigene therapy. Despite the importance of the triple helix, only limited high-resolution structural information is available. The x-ray crystal structure of the oligonucleotide d(GGCCAATTGG) is described; it was designed to contain the $d(G{\cdot}GC)_2$ fragment and thus provide the basic repeat unit of a DNA triple helix. Parameters derived from this crystal structure have made it possible to construct models of both parallel and antiparallel triple helices.

Combinations of three RNA or DNA strands produce triple helices that have been characterized in terms of base complementarity and the relative orientations of sugar-phosphate backbones (*1*). Hydrogen bonds are formed between the available functional groups of each base pair in a Watson-Crick double helix and those of the third (Hoogsteen) strand located in its major groove. The sequence recognition that this allows has been applied in the precise targeting of sequences in double-stranded DNA to exclude DNA binding proteins, including gene promoters (*2*), from their specific binding sites, and to direct single-site cleavage in chromosomal DNA (*3*). Triple helix formation has also been presented as a mechanism for alignment of homologous sequences before genetic recombination (*4*) and may take place in vivo (*5*).

Some conformational information about these species is available from spectroscopic studies in solution (6) and from fiber diffraction (7), but there is no parallel to the wealth of detailed crystallographic structural data obtained for oligonucleotide duplexes. The x-ray structure of a 2:1 peptide nucleic acid–DNA triplex has been reported (8), but crystals formed by nucleic acid triplexes are invariably disordered, at best giving rise to fiber-like diffraction (9). The crystal structure of the nonamer duplex $d(GCGAATTCG)_2$, analyzed previously by us, contained single G·GC triplets that resulted from molecular packing and provided an accurate picture of base-base interactions in a triple helix where the sugar-phosphate backbones of the purine-containing strands were in a parallel orientation (10). The 5′-terminal guanosine residues in that structure had no partners in the duplex for Watson-Crick base pairing and were free to interact in the crystal with an adjacent double helix. Examination of the molecular packing suggested that a second overhanging residue in a longer oligonucleotide could occupy a region of disordered solvent without disrupting the crystal lattice. This conformation would allow a further triplet to form and would generate a short but continuous section of triple helix.

The sequence selected for study was the decamer d(GGCCAATTGG); like the nonamer prototype, it crystallized as an 8–base pair (bp) regular B-form DNA (B-DNA) duplex. The unpaired 5′-terminal guanine bases of one strand (G11 and G12) stack beyond the end of the central duplex core and fit within the major groove of the abutting coaxial duplex (Fig. 1A). This produces a short stretch of G·GC triple helix with the purine strands parallel. However, the sequence-equivalent unpaired nucleotides (G1 and G2) of the other strand are twisted away from the stack (Fig. 1C) and rest in the major groove of an adjacent parallel duplex. The purine strand in this second triplex is antiparallel and constitutes a difference from the nonamer structure, which had parallel triplets at each end of the duplex (Fig. 1, B and D). The decamer structure thus contains examples of both parallel and antiparallel G·GC triple helices. Purine motif triplexes, triple helices in which most of the third-strand bases are purines, are found to have the purine-containing strands antiparallel when formed from nucleic acid fragments in solution (11), but have also been observed in the opposite orientation when the third strand was constrained in folded constructs where the component oligonucleotides were covalently linked (12). Recombination requires chains of similar sequence to have the same orientation in a three-stranded precursor of strand exchange (13).

The parallel and antiparallel regions are adjacent in the crystal structure (Figs. 1A and 2) and together make up the junction between three asymmetric units, $d(GGCCAATTGG)_2$. Continuity of base stacking between these regions appears to result from conformational adjustments at the end of the duplex, which increase the overlap between C3 and G1 of symmetry-related helices. This is achieved mainly through the large buckle and low propeller twist of the C4·G19 base pair.

The parallel triplets (Fig. 3A) are similar to those observed in the nonamer structure and are in good agreement with theoretical predictions (14). The Watson-Crick components of the triplets are undisturbed by the presence of the third base in that there is no significant opening and the mean H bond length is close to the standard value. Three hydrogen bonds are observed in a Hoogsteen pattern between the third strand guanines (denoted as G_H) and the Watson-Crick bases (denoted as G_{WC} and C_{WC}): between N2(G_H) and N7(G_{WC}), N1(G_H) and O6(G_{WC}), and O6(G_H) and N4(C_{WC}). The additional guanines thus span both bases of the Watson-Crick pair. The *x* displacement (15) of −2.52 Å (mean) is large compared with that of B-DNA (~−0.2 Å). Spectroscopic evidence suggests that such a displacement is a general feature of triplex formation (6) and is a consequence of accommodating the third strand within the major groove. Base alignments in both triplets deviate considerably from the mean planes, inclined at angles of up to 33.0° (mean 18.0°). The phenomenon may be associated to some extent with the position-

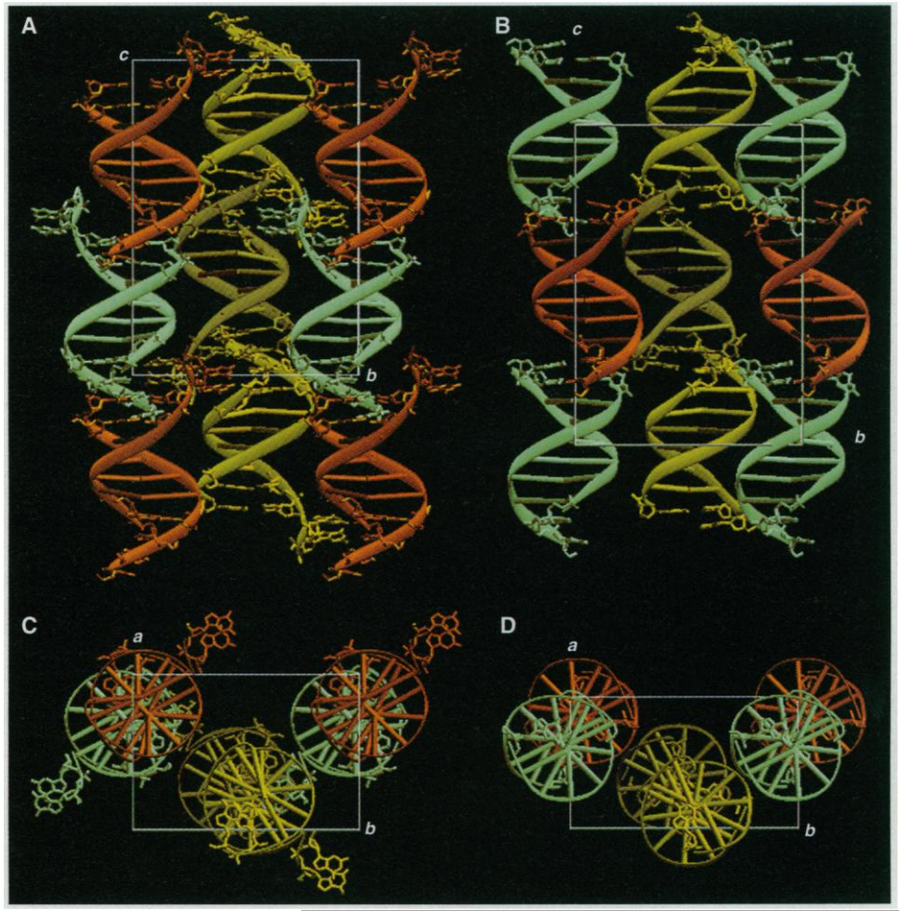

Fig. 1. Comparison of packing diagrams of the decamer and the nonamer [made with the program RIBBONS 2.4 (21)]. (**A**) Packing of decamer d(GGCCAATTGG) viewed down the crystallographic *a* axis. (**B**) Packing of nonamer d(GCGAATTCG) (4) viewed down the *a* axis. (**C**) Packing of the decamer viewed down the *c* axis. (**D**) Packing of the nonamer viewed down the *c* axis. Equivalent molecules are given the same color in both packings. Unit cells are represented as white boxes.

D. Vlieghe and L. Van Meervelt, Department of Chemistry, Katholieke Universiteit Leuven, Celestijnenlaan 200F, B-3001 Heverlee, Belgium.
A. Dautant, B. Gallois, G. Précigoux, Unité de Biophysique Structurale, EP CNRS, Université de Bordeaux II, 33405 Talence, France.
O. Kennard, Cambridge Crystallographic Data Centre, 12 Union Road, Cambridge CB2 1EZ, UK.
*To whom correspondence should be addressed.

al adjustments noted above for optimization of stacking between successive bases near the junction of the parallel and antiparallel triplexes, but is also an indication of flexibility comparable to the propeller twisting observed in Watson-Crick base pairs. The helical twist is 29.1° and the rise 3.20 Å. All bases are *anti* relative to their sugars. Five of the six sugar puckering modes are in the normal B-DNA range between C1′-*endo* and C2′-*endo*, whereas one sugar (C3) adopts a C4′-*exo* conformation typical of A-DNA.

The purine strands of the second triple helix have an antiparallel orientation (Fig. 3B) and a reverse-Hoogsteen hydrogen bond pattern between G_H and only G_{WC} of the Watson-Crick pair. There are two hydrogen bonds: between N7(G_{WC}) and N1(G_H), and between O6(G_{WC}) and N2(G_H). Again, the geometry of the Watson-Crick pairing is similar to that in a double helix. The bases of the triplets are even more tilted than in the parallel triple helix (mean value of 20.6°). In the G2·G9C14 triplet, a third, weak C-H···O hydrogen bond (3.33 Å) is formed between C8(G_{WC}) and O6(G_H). Interbase C-H···O hydrogen bonds have been described in other oligonucleotide structures (*16*). The helical parameters are generally comparable to those in the parallel triple helix, with a large mean *x* displacement (−1.52 Å), a helical twist of 29.5°, and a rise of 3.27 Å. The backbone parameters are in the normal range for B-DNA except for the γ angle of G2, which is in the *trans* conformation rather than (+)-*gauche*. The glycosidic angles are *anti*. Sugar puckers are in the C2′-*endo* range, except for that of C13, which is C3′-*endo*. The sugar-phosphate backbones of the Hoogsteen strands of both triplexes occupy similar positions in the major groove, despite the different modes of hydrogen bonding in each between the Watson-Crick pair and the third base.

Although reliable theoretical models are available for both parallel and antiparallel G·GC triplets (*14*, *17*), construction of an extended triplex requires that the twist and rise between successive steps be known. The present structure provides these helical parameters, as well as the base triplets themselves, and has allowed models of both parallel and antiparallel G·GC triple helices to be generated. The rise and twist of the antiparallel fragment were replicated by aligning the G2-G9C14 triplet (sugars and bases) through least-squares fitting onto the G1·G10C13 triplet of a second unit. The nucleotide residues of the latter were removed and the process repeated until the desired length of sequence was obtained. Minor deviations from standard phosphate geometry were corrected by molecular mechanics minimization (*18*). The G2·G9C14 unit was chosen in preference to G1·G10C13 because the former is less likely to be influenced by proximity to the parallel triplet region. The parallel helix was generated in an analogous manner through use of G11·G19C4 as the unit of repeat. The resulting $(G{\cdot}GC)_{12}$ triple helices are illustrated in Fig. 4. The antiparallel $(G{\cdot}GC)_{12}$ triplex has a twist of 29.5° and a rise of 3.45 Å, Crick-Hoogsteen and Watson-Hoogsteen groove widths are ~7 and ~3 Å, respectively. In the parallel triplex, twist is 26.8° and rise 3.70 Å, whereas the widths of the two grooves are similar (Crick-Hoogsteen, ~6 Å; Watson-Hoogsteen, ~7 Å). A second pair of triplexes generated independently with the helix-building program MORCAD (*19*), which extracts the required parameters and triplet geometry directly from the x-ray structure, gave similar results [root mean

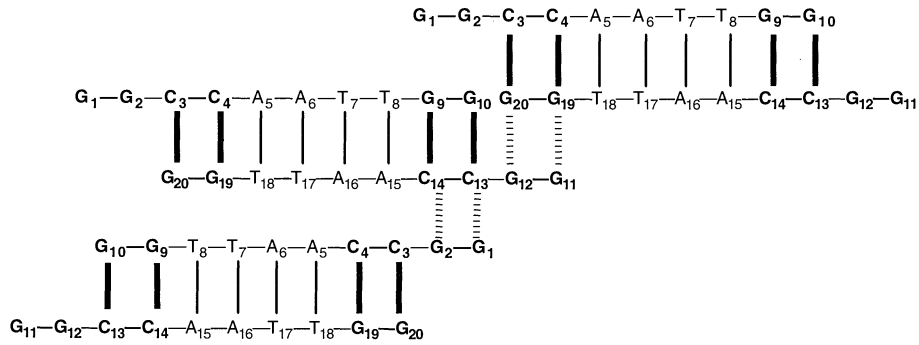

Fig. 2. Representation of triplex formation as a consequence of crystal packing for the decamer d(GGCCAATTGG). The decamer was synthesized by solid-phase phosphoramidite methods and crystallized from a buffered 0.4 mM solution of DNA (pH = 6.0) containing 43 mM $MgCl_2$, 0.6 mM spermine, and 3% 2-methyl-2,4-pentanediol (MPD) and equilibrated against 40% MPD by the vapor diffusion technique at 16°C. The space group is $P2_12_12_1$ with *a* = 26.25, *b* = 36.82, and c = 53.23 Å, and one duplex per asymmetric unit. The x-ray intensities to 2 Å were collected from a single crystal of dimensions 0.05 by 0.1 by 0.05 mm on the LURE D41 beamline (Paris) with an MAR Research image plate at room temperature. A total of 12,303 reflections were measured and reduced to 3534 unique reflections (R_{sym} = 4.6%, completeness 94.6%, multiplicity 3.0) with the IPMOSFLM program (*22*) and the CCP4 package (*23*). Molecular replacement techniques were applied for solving the structure with the central octamer of d(GCGAATTCG) (*10*) with the AMoRe program (*24*). The overhanging bases were added during visualization of the electron density maps. Refinement on F^2 with SHELXL-93 (*25*) reduced the *R* factor to 20.2% for the 3212 reflections ($F > 4\sigma F$) between 10 and 2 Å (*wR2* = 0.52), including 44 water molecules. The central d(CCAATTGG) adopts a B-DNA conformation with an average helical twist of 35.5° and a rise of 3.49 Å. Triple helix parameters were calculated with the Curves program (*26*); only the Watson-Crick bases of the triplexes (fitted to standard geometry) were used to determine the helix axis. Final coordinates are deposited in the Brookhaven Protein Data Bank (*27*) and the Nucleic Acid Data Bank (*28*) (UDJ049).

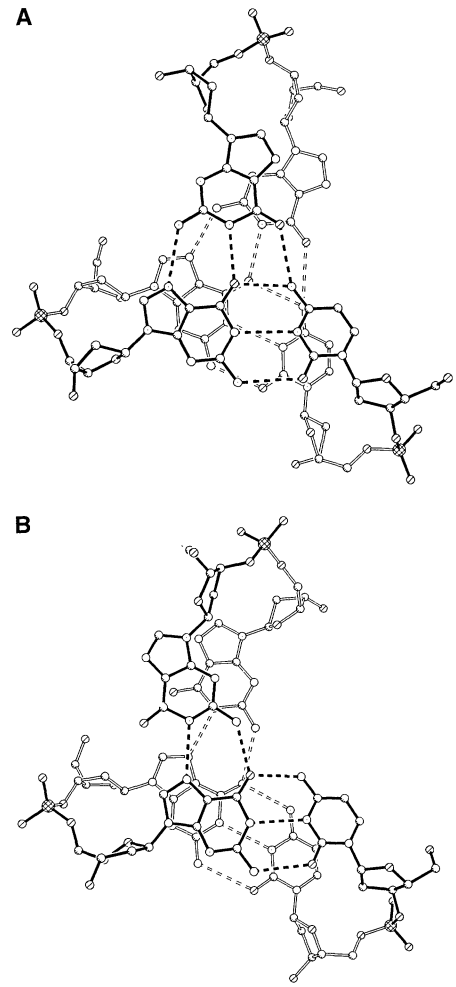

Fig. 3. Representations of the triple helices present in the crystal structure of d(GGCCAATTGG). Ball-and-stick representations of (**A**) the parallel triple helix and (**B**) the antiparallel triple helix. Mean hydrogen bond lengths are as follows: 2.93 Å for the Hoogsteen base pairing (ranging from 2.72 to 3.29 Å) and 2.92 Å for the Watson-Crick base pairing (ranging from 2.79 to 3.05 Å) in the parallel triple helix, and 2.80 Å for the Hoogsteen base pairing (ranging from 2.65 to 2.89 Å) and 2.94 Å for the Watson-Crick base pairing (ranging from 2.81 to 3.13 Å) in the antiparallel triple helix.

square (rms): 1.21 Å antiparallel, 1.80 Å parallel].

Only limited conformational information is presently available for triple helices. The two families, identified as purine and pyrimidine motifs, have been shown generally to be right handed, with the Watson and Crick portion resembling B-DNA. The third strand occupies part of the major groove and all nucleoside residues typically have *anti*-glycosidic conformations and C2′-*endo* sugar puckers (*1*). Structural detail is sparse in the case of purine-purine-pyrimidine (R·RY) triplexes and has been reported only for examples where the purine strands are antiparallel (*11*, *20*). Comparison with our model is complicated by the fact that G·GC, A·AT, and T·AT triplets in the purine motif are not isosteric, giving rise to sequence-dependent variations in the conformations of the mixed sequences studied experimentally. A single published study in which nuclear magnetic resonance spectroscopy was used (*20*) is in broad agreement with our results and indicated similar conformations for the nucleoside residues. This restrained molecular dynamics experiment produced an ensemble of similar structures, making numerical comparison of parameters difficult. Helical twist and rise at G-G steps were ~35° and ~3.8 Å, respectively, and compare with 29° and 3.6 Å for the present antiparallel model. Interproton nuclear Overhauser effect connectivities at G-G steps in the Hoogsteen strand were found to be weak and are consistent with the relevant distances between idealized hydrogen atom positions calculated for our structure (*18*). Separations in the third strand between H8 of one residue and H1′, H2′, H2″, and H8 of its 5′ neighbor were in the same relative order as in the Watson-Crick strands but, with the exception of the first of these, were on average 30% greater.

The x-ray structure of the DNA nonamer d(GCGAATTCG) presented an opportunity for crystallographic examination of short sections of parallel triple helix through modification of that nucleotide sequence. The resulting x-ray structure, which we describe, contained the predicted dinucleotide fragment of parallel R·RY triplex suitable for extension into an infinite triple helix. The crystals unexpectedly also contained a second antiparallel triplex region. Both portions of the structure have been elaborated into models that are based almost entirely on high-resolution crystallographic data. Separately, these provide starting points for describing the properties of triple helices in molecular terms; for example, in terms aimed at developing strategies for enhancing triplex stability. The success of the method indicates that further sequence modifications could give access to three-dimensional structures of other triple helix motifs for which more direct experimental approaches have proved consistently unproductive.

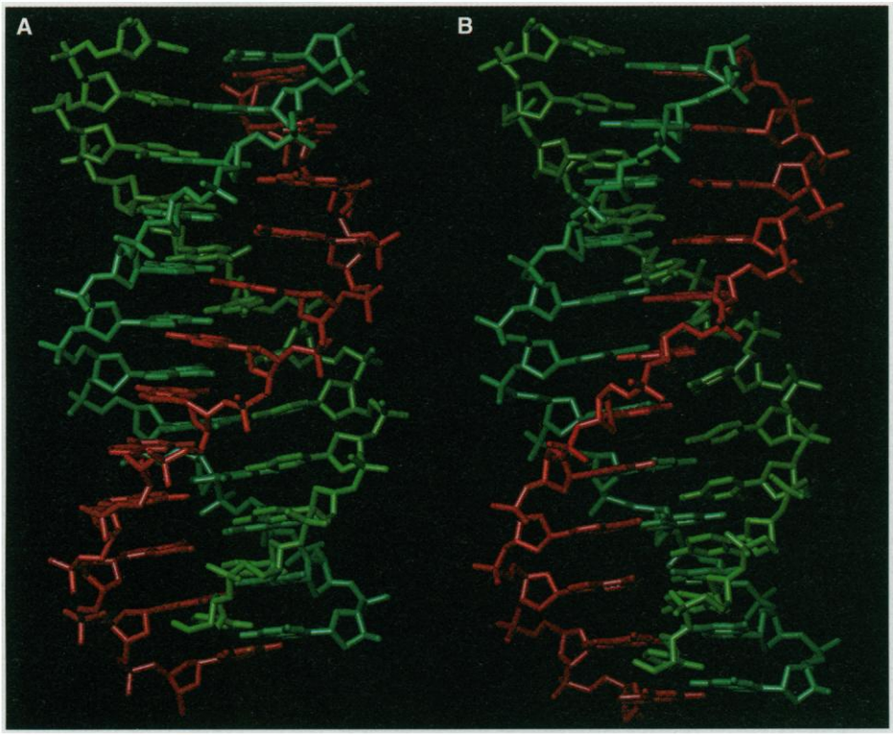

Fig. 4. View into the major groove occupied by the third strand of the (**A**) antiparallel and (**B**) parallel $(G{\cdot}GC)_{12}$ triple helix models generated by least-squares fitting of the triplets of the $(G{\cdot}GC)_2$ triplexes observed in the crystal structure of d(GGCCAATTGG). Both Watson-Crick strands are green and the third G strand is red. Coordinates are available from the Nucleic Acid Data Bank upon request (M1UDJ049, parallel; M2UDJ049, antiparallel).

REFERENCES AND NOTES

1. P. B. Dervan, *Nature* **359**, 87 (1992); J.-S. Sun and C. Hélène, *Curr. Opin. Struct. Biol.* **3**, 345 (1993); M. D. Frank-Kamenetskii and S. M. Mirkin, *Annu. Rev. Biochem.* **64**, 65 (1995).
2. L. J. Mahler, B. Wold, P. B. Dervan, *Science* **245**, 725 (1989); G. Duval-Valentin, N. T. Thuong, C. Hélène, *Proc. Natl. Acad. Sci. U.S.A.* **89**, 504 (1992); M. Cooney, G. Czernuszewicz, E. M. Postel, S. J. Flint, M. E. Hogan, *Science* **241**, 456 (1988).
3. S. A. Strobel, L. A. Doucette-Stamm, L. Riba, D. E. Housman, P. B. Dervan, *Science* **254**, 456 (1991).
4. P. Hsieh, C. S. Camerini-Otero, R. D. Camerini-Otero, *Genes Dev.* **4**, 1951 (1990); B. J. Rao and C. M. Radding, *Proc. Natl. Acad. Sci. U.S.A.* **91**, 6161 (1994).
5. Y. Kohwi, S. R. Malkhosyan, T. Kowhi-Shigematsu, *J. Mol. Biol.* **223**, 817 (1992).
6. I. Radhakrishnan and D. J. Patel, *Biochemistry* **33**, 11405 (1994).
7. S. Arnott and E. Selsing, *J. Mol. Biol.* **88**, 509 (1974); G. Raghunathan, H. T. Miles, V. Sasisekharan, *Biochemistry* **32**, 455 (1993).
8. L. Betts, J. A. Josey, J. M. Veal, S. R. Jordan, *Science* **270**, 1838 (1995).
9. K. Liu, H. T. Miles, K. D. Parris, V. Sasisekharan, *Nature Struct. Biol.* **1**, 11 (1994).
10. L. Van Meervelt *et al.*, *Nature* **374**, 742 (1995).
11. P. A. Beal and P. B. Dervan, *Science* **251**, 1360 (1991).
12. A. K. Shchyolkina *et al.*, *FEBS Lett.* **367**, 81 (1995).
13. V. B. Zhurkin, G. Raghunathan, N. B. Ulyanov, R. D. Camerini-Otero, R. L. Jernigan, *J. Mol. Biol.* **239**, 181 (1994).
14. S.-P. Jiang, R. L. Jernigan, K.-L. Ting, J. L. Syi, G. Raghunathan, *J. Biomol. Struct. Dyn.* **12**, 383 (1994).
15. S. Diekmann, *EMBO J.* **8**, 1 (1989).
16. G. A. Leonard, K. McAuley-Hecht, T. Brown, W. N. Hunter, *Acta Crystallogr. D* **51**, 136 (1995).
17. J. M. Piriou, C. Ketterlé, J. Gabarro-Arpa, J. A. H. Cognet, M. Le Bret, *Biophys. Chem.* **50**, 323 (1994).
18. A. T. Brünger. *X-PLOR Version 3.1. A System for X-Ray Crystallography and NMR* (Yale Univ. Press, New Haven, CT, 1992).
19. M. Le Bret, J. Gabarro-Arpa, J. C. Gilbert, C. Lemaréchal, *J. Chim. Phys. Phys. Chim. Biol.* **88**, 2489 (1991).
20. I. Radhakrishnan and D. J. Patel, *Structure* **1**, 135 (1993).
21. M. Carson, *J. Appl. Cryst.* **24**, 958 (1991).
22. A. G. W. Leslie, in *Crystallographic Computing 5*, D. Moras, A. D. Podjarny, J. C. Thierry, Eds. (Oxford Univ. Press, New York 1991), pp. 50–61.
23. Collaborative Computational Project, No. 4, *Acta Crystallogr. D* **50**, 760 (1994).
24. J. Navaza, *Acta Crystallogr. A* **50**, 157 (1994).
25. G. M. Sheldrick, *SHELXL-93. Program for Crystal Structure Refinement* (University of Göttingen, Göttingen, Germany, 1993).
26. R. Lavery and H. Sklenar, *J. Biomol. Struct. Dyn.* **6**, 655 (1989).
27. F. C. Bernstein *et al.*, *J. Mol. Biol.* **112**, 535 (1977).
28. H. M. Berman *et al.*, *Biophys. J.* **63**, 751 (1992).

29. Supported by the Research Council of the Catholic University, Leuven (Belgium), the Flemish Institute for the Benefit of Scientific and Technological Research in Industry (IWT), the CNRS (France), the British Medical Research Council, and the National Fund for Scientific Research (Belgium) (L.V.M.). We thank A. Bentley and R. Fourme for help with data collection at LURE, Paris; B. Langlois d'Estaintot for handling the crystal; S. A. Salisbury for help with the preparation of the manuscript; and H. Reynaers for continued support.

24 April 1996; accepted 19 July 1996